energies

MDPI

Article

An Assessment of Replacing Aluminum Tubes Hosting Nuclear Fuels with Stainless Steel in a Subcritical Nuclear Reactor

Diego Medina-Castro [1], Héctor René Vega-Carrillo [2], Antonio Baltazar-Raigosa [2,3], Tzinnia Gabriela Soto-Bernal [4], Régulo López-Callejas [1] and Benjamín Gonzalo Rodríguez-Méndez [1,*]

[1] Plasma Physics Laboratory, National Institute for Nuclear Research, Carretera México-Toluca S/N, Ocoyoacac 52750, Mexico; diego.medina@inin.gob.mx (D.M.-C.); regulo.lopez@inin.gob.mx (R.L.-C.)
[2] Radiobiology Academic Group, Academic Unit for Nuclear Studies, Autonomous University of Zacatecas, Cipres 10, Fracc. La Peñuela, Zacatecas 98068, Mexico; rvega@uaz.edu.mx (H.R.V.-C.); raigosa.antonio@uaz.edu.mx (A.B.-R.)
[3] Electrical Engineering Academic Unit, Autonomous University of Zacatecas, Av. Lopez Velarde s/n. Col. Centro, Zacatecas 98000, Mexico
[4] School of Engineering and Sciences, Tecnologico de Monterrey, Av. Eugenio Garza Sada 1500, Aguascalientes 20328, Mexico; tzinnia.soto@tec.mx
* Correspondence: benjamin.rodriguez@inin.gob.mx

Abstract: This computational study using MCNP5 evaluated the feasibility of replacing 6061-T6 aluminum with 316L stainless steel (SS-316L) for the tubes hosting the uranium slugs in the subcritical nuclear reactor Nuclear Chicago model 9000, thereby contributing to its preservation as a key resource for nuclear research and education in Mexico. Simulations and dosimetric analyses (ICRP/ICRU) confirmed subcriticality in both configurations. Notably, SS-316L demonstrated an effective attenuation of peripheral gamma radiation and a reduction in the ambient neutron dose, indicating a considerable improvement in radiological safety. Although a reduction in thermal and epithermal neutron fluence was observed, the similarity in the gamma spectrum suggests no significant alteration for gamma spectroscopic experiments. In conclusion, SS-316L presents a promising alternative that enhances radiological safety and reactor longevity, making it a worthy consideration as a replacement material. Further experimental investigation is recommended to assess material activation and the gamma dose in the vicinity of the fuel.

Keywords: subcritical reactor; tubes for fuel slugs; Monte Carlo; effective multiplication factor; spectrometry and dosimetry

check for updates

Academic Editor: Gediminas Stankūnas

Received: 16 May 2025
Revised: 6 June 2025
Accepted: 17 June 2025
Published: 19 June 2025

Citation: Medina-Castro, D.; Vega-Carrillo, H.R.; Baltazar-Raigosa, A.; Soto-Bernal, T.G.; López-Callejas, R.; Rodríguez-Méndez, B.G. An Assessment of Replacing Aluminum Tubes Hosting Nuclear Fuels with Stainless Steel in a Subcritical Nuclear Reactor. *Energies* **2025**, *18*, 3213. https://doi.org/10.3390/en18123213

Copyright: © 2025 by the authors. Licensee MDPI, Basel, Switzerland. This article is an open access article distributed under the terms and conditions of the Creative Commons Attribution (CC BY) license (https://creativecommons.org/licenses/by/4.0/).

1. Introduction

A nuclear reactor is a machine that contains an arrangement of nuclear fuel designed to generate and control nuclear fission. Reactors are primarily classified into two types: power reactors, which are designed for electricity generation, and research reactors, which are utilized for a wide range of scientific studies and technological applications in the nuclear field [1–3]. Another fundamental distinction lies between critical reactors, which can sustain a self-sustained chain reaction, and subcritical reactors, which require an external neutron source to maintain fission processes, an inherent characteristic that increases their operational safety [4,5].

At the global level, subcritical research reactors play a crucial role. Since they do not sustain a self-sustained nuclear chain reaction, they offer an inherently safer environment for experimentation; the production of radioisotopes for medical, industrial, and agricultural applications; non-destructive material analysis using neutron techniques; and

the training of future generations of professionals in nuclear engineering and related sciences [6–11].

In Mexico, there are two subcritical nuclear reactors of the Nuclear Chicago model 9000 (NC-9000): one reactor is located at the National Polytechnic Institute (IPN), and another is at the Autonomous University of Zacatecas (UAZ). These reactors are primarily used for teaching, hands-on training, and limited scientific research [5,12]. The tubes that house the fuel rods in these reactors were manufactured using 6061-T6 aluminum alloy (Al-6061-T6; Alcoa, Pittsburgh, PA, USA), selected for its low neutron capture cross-section and good mechanical strength.

However, this alloy has limited corrosion resistance within the reactor environment, especially under radiation exposure and prolonged contact with light water (used as a moderator and reflector), which tends to evaporate and concentrate mineral salts and other compounds [5,13]. These processes contribute to corrosion in the tubes that host the uranium slugs [14]. Previous studies have confirmed the tendency of Al-6061-T6 to form oxides under prolonged operational conditions and in the presence of impure water, compromising its structural integrity and, potentially, its heat transfer properties [13,15,16]. This situation highlights the necessity of investigating alternative materials to extend the service life of the reactor, ensure its safe and continuous operation, and maintain neutron and gamma spectral characteristics, as well as radiation dose levels, within acceptable limits for its application in education and research [13,17].

In response to this challenge, the present study evaluates 316L stainless steel (SS-316L) as an alternative material for the tubes hosting the fuel slugs. While it is well known that SS-316L has a significantly higher neutron absorption cross-section than aluminum, an apparent disadvantage for a core component, there are multifactorial motivations that justify its consideration as a viable and potentially superior long-term candidate. First, the primary failure mechanism of the current material is corrosion, an area in which SS-316L offers improved resistance, especially in aqueous environments and under irradiation. This improved durability is crucial for extending the lifespan of components, reducing the frequency of maintenance and its associated expenses, and minimizing the risk of failures that could compromise reactor safety or operational readiness. Secondly, SS-316L demonstrates better mechanical properties than Al-6061-T6, such as increased tensile strength and toughness, which could improve the structural integrity of the fuel assembly. Thirdly, while its neutron absorption rate is greater, it is vital to measure the precise effect on the neutron fluence spectrum and dosimetric parameters within the NC-9000 subcritical nuclear reactor (Nuclear-Chicago Corporation, Des Plaines, IL, USA). Given the specific characteristics of this low-power reactor and its application in education and fundamental research, it is reasonable to conclude that the neutronic impact remains acceptable and is offset by the improved lifespan and reliability of the material.

Therefore, the primary objective of this study is to conduct a comprehensive comparison between the performance of Al-6061-T6, the current material for housing tubes, and SS-316L as an alternative material for the housing tubes that contain the fuel slugs of the NC-9000 nuclear reactor. Through detailed Monte Carlo simulations using version 5 of the MCNP code [18,19] and dosimetric analyses based on the International Commission on Radiological Protection (ICRP) and the International Commission on Radiation Units and Measurements (ICRU) recommendations, their behavior is evaluated regarding the effective multiplication factor, neutron spectrum, neutron fluence, and radiation dosimetry. This research aims to determine whether the advantages of SS-316L as a potential substitute, particularly its superior corrosion resistance and mechanical properties, can provide a more sustainable and safer solution while maintaining essential neutronic properties within acceptable limits for the efficient operation of the reactor. Such a result would represent a

significant step toward preserving this key resource for nuclear research and education in Mexico and all those sites around the world with this type of subcritical nuclear reactor experiencing corrosion problems in the aluminum tubes.

2. Methodology

2.1. Reactor

The subcritical reactor modeled in this study is the NC-9000 reactor, characterized by a core containing 270 fuel tubes arranged in a compact hexagonal lattice, as shown in the three-dimensional view in Figure 1. The center-to-center spacing between these tubes is 4.445 cm. Each tube, with a diameter of 3.18 cm and a length of 149.86 cm, contains hollow cylindrical slugs of natural uranium. Each tube consists of a lower section filled with light water, a middle section housing the uranium fuel slugs, and an upper section containing air (Figure 2).

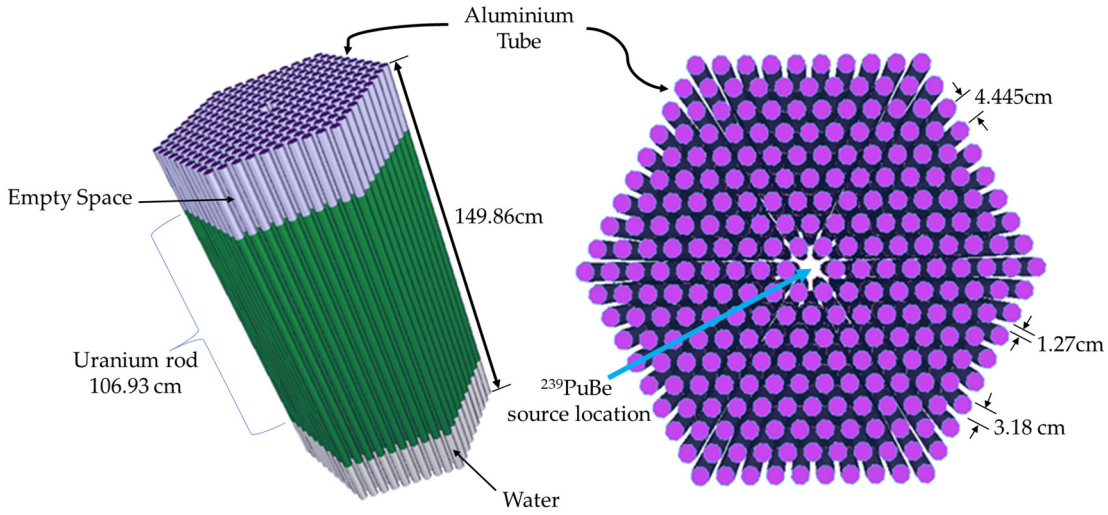


Figure 1. A three-dimensional view of the NC-9000 subcritical reactor showing the hexagonal array of 270 fuel tubes. The core has a maximum diameter of approximately 88.9 cm. The central ^{239}PuBe neutron source is located at the center of the core. Each fuel tube contains natural uranium slugs surrounded by light water, which serves as both a moderator and a reflector.

Subcritical reactors require an external neutron source; in this case, the source is a plutonium–beryllium (^{239}PuBe) neutron source located at the center of the core. The source strength is 1.11×10^7 n/s and has a nominal activity of 0.185 TBq [20], playing a crucial role in sustaining the criticality of the subcritical system. The simulations were performed assuming this nominal activity remains constant. However, in actual reactor operation, the gradual decrease in source activity due to radioactive decay is considered during periodic evaluations. This is particularly relevant for experimental planning and dose estimation, especially in training sessions and detector-based measurements where source intensity influences fluence and exposure time. Figure 2 also shows the spatial location of the virtual detectors used in the simulations, with their specific positional characteristics (coordinates and orientation) detailed in Table 1.

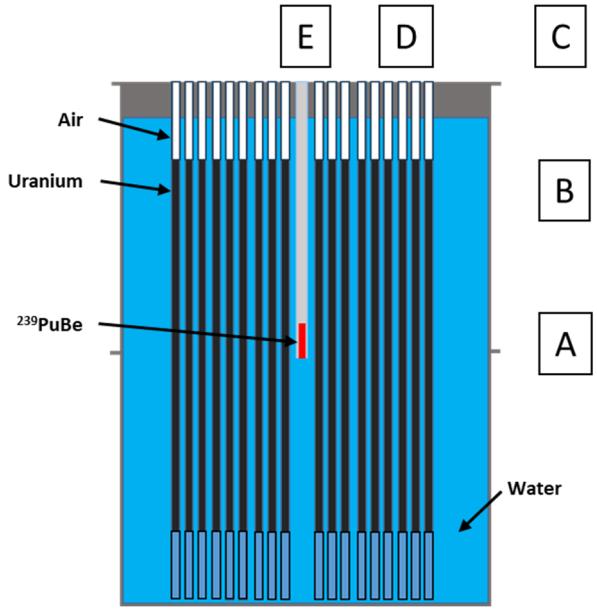


Figure 2. An isometric view of the NC-9000 reactor in MCNP5, where the letters A, B, C, D, and E indicate the positions of the virtual detectors used in the simulations.

Table 1. The location and purpose of the point detectors used in the simulations.

Identifier	Location (x, y, z) [cm]	Point Description
Position A	(71.0, 0.0, 73.3)	Lateral to the reactor, near-core position
Position B	(71.0, 0.0, 111.9)	Lateral to the reactor, elevated position along the vertical axis
Position C	(60.0, 0.0, 162.5)	Top of the reactor, experimental handling area
Position D	(25.0, 0.0, 162.5)	Upper intermediate section, near instructional and student access areas
Position E	(0.0, 0.0, 162.5)	Center of the reactor top, a typical area for experimental practice

2.2. Source and Virtual Detector Modeling

Virtual F5 detectors (used to calculate point fluence) were placed at strategic locations around the core, specifically at lateral and top positions, representing areas frequently accessed during training sessions.

Each virtual detector was modeled using the MCNP5 F5 tally (Los Alamos National Laboratory, Los Alamos, NM, USA), which provides point-specific fluence for both neutrons and gammas. These detectors are defined as zero-volume spheres with perfect energy resolution and no physical perturbation of the system. The detector orientations were selected to simulate typical positions accessed during training and experimental procedures. They were placed both laterally and vertically relative to the core to capture variations in influence and energy spectrum with distance and shielding. Their locations and coordinates are detailed in Table 1.

The goal was to obtain neutron and photon spectra and calculate the absorbed dose in these regions. The conversion from particle fluence to ambient equivalent dose was carried out using H*(10) conversion coefficients for neutrons and photons, by the recommendations established in ICRP Publication 74 [21] and the factors proposed in ICRU Report 95 [22], which define a new operational quantity for ambient dose equivalent (H*).

The coefficients applied correspond to energy-dependent fluence-to-dose conversion factors for H*(10). For neutrons, values range from 2 to 300 pSv·cm^2 per neutron depending on the energy group, while for photons, values vary from approximately 0.01 to 1.5 pSv·cm^2

per photon. The energy binning in the simulations was matched to the available conversion tables, ensuring consistency with international dosimetric standards.

2.3. Computational Model

The computational model of the NC-9000 reactor was implemented in MCNP5 (ver. MCNP5-1.60) based on technical design specifications and the literature as reported by Papastefanou [4]. The geometry includes a hexagonal arrangement of 270 fuel tubes with a center-to-center spacing of 4.445 cm. Each tube has an outer diameter of 3.18 cm and a wall thickness of 0.89 mm, containing five cylindrical slugs of natural uranium (2.77 cm in diameter), separated by light water. These details now reflect a more complete and reproducible modeling approach. A similar three-stage simulation methodology combining MCNP-based transport with nuclide evolution codes was previously applied in the HELIOS experiment, as reported by Oettingen et al. [23]. The neutron source was a central ^{239}PuBe source, with an emission rate of 1.11×10^7 n/s, modeled using a typical (α,n) energy distribution based on experimental data.

Materials were defined using the ENDF/B-VII.1 nuclear data library (Brookhaven National Laboratory, Upton, NY, USA). Specific material compositions include Al-6061-T6 for the reference cladding, SS-316L for the alternative case, natural uranium metal (U), light water as the moderator and reflector, and Lucite for structural elements. Densities were taken from technical documentation and adjusted to maintain consistency in the physical modeling.

To evaluate the feasibility of replacing the current Al-6061-T6 housing tubes with SS-316L stainless steel, detailed simulations using MCNP5 were performed to compare the influence of the tube material on neutron and gamma spectroscopy and dosimetry, hosting the uranium fuel slugs [24,25]. For this purpose, a three-dimensional model of the NC-9000 reactor geometry was developed based on the dimensions and arrangement shown in Figures 1 and 2, including the central neutron source and the hexagonal arrangement of fuel tubes. Neutron and photon transport was simulated using the ENDF/B-VII.1 nuclear data cross-section libraries. To ensure adequate statistical convergence, 10^8 particle histories were simulated, and convergence was assessed using the relative variance histograms generated by MCNP5.

2.4. Evaluated Scenarios

Two scenarios were investigated: tubes with the conventional Al-6061-T6 housing tube and another scenario using the proposed SS-316L stainless-steel housing tube. For each scenario, the effective multiplication factor (k_{eff}) was estimated using the KCODE card in MCNP5, confirming the subcritical condition ($k_{eff} < 1$).

The same cladding thickness (0.89 mm) was used for both Al-6061-T6 and SS-316L in the simulations. This approach ensured a fair geometrical comparison that isolates the effect of the material properties on neutron moderation and absorption. Nevertheless, we acknowledge that using a thinner SS-316L cladding could be a practical strategy to mitigate neutron attenuation. This possibility is highlighted in the conclusions as a promising direction for future optimization studies focused on improving the reactor's neutronic performance while preserving structural benefits.

In addition, the spectra were estimated, and the doses were calculated in positions A, B, C, D, and E (Figure 2) to assess the impact of the housing tube material on the spatial and energy distribution of neutrons and gamma rays. This provides essential information for determining the potential superiority of SS-316L as an alternative material in terms of radiological safety, structural integrity, and performance for research and educational purposes, particularly when compared to the known limitations of Al-6061-T6.

Table 2 presents a detailed comparison of the most relevant properties of Al-6061-T6 and SS-316L, focusing on their behavior under oxidation and corrosion processes in subcritical reactor operating conditions. This comparison highlights the limitations of Al-6061-T6, particularly its susceptibility to corrosion induced by mineral content in reactor water and its accelerated degradation under irradiation. In contrast, SS-316L offers significant advantages, including a higher melting point, a lower thermal expansion coefficient, and the formation of a stable, self-healing passive layer that provides superior protection against oxidation and greater structural durability. As quantitatively demonstrated in Table 2, these properties confirm SS-316L as a viable and superior alternative to the current housing tube material, improving operational reliability while significantly extending the system service life.

Table 2. Comparison of relevant housing tube properties related to oxidation resistance.

Key Property Related to Oxidation	Al-6061-T6	SS-316L	Implications in Corrosive Environments
Density (g/cm^3)	2.70	8.00	Steel is denser but provides greater structural integrity.
Melting Point (°C)	582–651	1375–1400	Steel has higher resistance to elevated temperatures.
Corrosion Resistance	Good in neutral environments, weak in the presence of chlorides or minerals	Excellent in humid and radioactive environments	Superior durability to Al-6061-T6 in contact with mineralized water
Surface Oxide	Forms Al_2O_3, less stable in irradiated environments	Forms Cr/Fe/Ni oxides, self-passivating and stable	The formation of a Cr-rich passive layer in SS-316L provides notable corrosion resistance.
Thermal Conductivity (W/m·K)	167	14.6	Al-6061-T6 dissipates heat more effectively, but its performance is compromised by oxidation.
Thermal Expansion Coefficient ($\times 10^{-6}$/K)	23.6	16.0	Al-6061-T6 expands more, increasing the likelihood of cracking.
Tensile Strength (MPa)	310	485	Steel provides greater mechanical strength.
Yield Strength (MPa)	276	170	Al-6061-T6 deforms less before yielding, but is more prone to fatigue.
Behavior Under Irradiation	Accelerated oxide degradation and microcrack formation	High-dimensional stability	SS-316L addresses the accelerated degradation and microcracking observed in Al-6061-T6 under irradiation.
Oxidation Resistance in Reactor Water	Mineral deposits, embrittlement, and wall thinning were observed	High resistance to oxidation with minerals and radiation	SS-316L is the most resilient long-term candidate.

The thermal neutron absorption cross-sections of the constituent elements can also explain the differences in neutron attenuation. Aluminum has a relatively low absorption cross-section (0.231 barns), while stainless-steel components exhibit significantly higher

values: iron (2.56 barns), chromium (3.05 barns), and nickel (4.49 barns). These differences account for the more pronounced reduction in neutron fluence observed with SS-316L.

2.5. Data Analysis and Convergence Criteria

To analyze the influence of materials on radiation attenuation, the exponential attenuation law was applied ($I(x) = I_0{}^{-\mu x}$), where I_0 is the initial radiation intensity, $I(x)$ is the intensity after passing through a thickness x, and μ is the attenuation coefficient for neutrons and photons, obtained from the ENDF/B-VII.1 database [26,27] for the relevant energies in the simulated neutron and gamma spectra of the reactor. Statistical convergence of the simulations was ensured by simulating 10^8 particle histories. Convergence was assessed using the relative variance histograms generated by MCNP5 to confirm that the results met acceptable uncertainty levels, all of which were below 5%, ensuring reliable analysis.

The attenuation coefficients (μ) were calculated from the effective macroscopic cross-sections ($\sum$) derived from ENDF/B-VII.1 libraries. For thermal neutrons ($\approx$0.025 eV), typical macroscopic absorption cross-sections are approximately 0.007 cm^{-1} for Al-6061-T6 and 0.035 cm^{-1} for SS-316L. For fast neutrons ($\approx$1 MeV), the values are $\approx$0.002 cm^{-1} and $\approx$0.015 cm^{-1}, respectively. For photons of 1 MeV, the linear attenuation coefficients are $\approx$0.060 cm^{-1} for aluminum and $\approx$0.280 cm^{-1} for SS-316L. These values were used to interpret differences in neutron and photon fluence attenuation across scenarios.

3. Results and Discussion

This section details the findings of simulations performed using the MCNP5 code, emphasizing the evaluation of how different materials for the fuel slug housing tubes influence the reactor's neutronic, gamma, and criticality properties (k_{eff}). These analyses encompass detailed spectral distributions of neutrons and gamma rays in key areas, k_{eff} values (calculated based on the parameters outlined in the methodology), and gamma and neutron dose rates at strategic locations. These results facilitate a direct comparison between the conventional Al-6061-T6 housing tube and the proposed SS-316L stainless-steel alternative, with the aim of highlighting the potential of the latter to optimize reactor operation and improve its safety.

3.1. Effective Multiplication Factor (k_{eff})

The effective multiplication factor (k_{eff}) [28], a critical parameter for reactor safety, was calculated for both scenarios: the reactor modeled with Al-6061-T6 and SS-316L tubes hosting the same fuel slugs. For Al-6061-T6, k_{eff} was 0.83022 $\pm$ 0.00005, while for the proposed SS-316L housing tube, the value obtained was 0.7052 $\pm$ 0.0001. Both values are below unity ($k_{eff} < 1$), confirming the inherently subcritical nature of the reactor and ensuring a wide margin of operational safety regardless of the housing tube material. Using Al-6061-T6 tubes, k_{eff} was 17.73% larger than the k_{eff} obtained with SS-316L tubes; this was due to the higher neutron absorption cross-section of stainless-steel components (mainly Fe, Cr, and Ni) compared to aluminum. Although this intrinsic property of SS-316L leads to lower overall core reactivity, it further reinforces the deeply subcritical condition of the system, an added advantage from the standpoint of passive safety, without negatively affecting the viability of experimental activities that rely on the external neutron source.

3.2. Neutron Spectra

The analysis of neutron spectra at positions A, B, C, D, and E (Figure 3) reveals significant variations in neutron fluence (Φ), depending on both the housing tube material (Al-6061-T6 or SS-316L) and the measurement geometry. At position A (Figure 3a), Al-6061-T6 consistently exhibits a higher neutron fluence across the entire energy spectrum than SS-316L. This material (Al-6061-T6) also shows a spectrum with a greater proportion

of neutrons in the thermal region. These observations are attributed to the fact that Al-6061-T6 has a lower neutron absorption cross-section than SS-316L and acts as a more efficient moderator, facilitating neutron thermalization and transport. In contrast, SS-316L, characteristically due to the higher absorption cross-sections of its components (Fe, Cr, Ni), reduces the neutron fluence; specifically, at position A, the thermal neutron fluence (<0.1 eV) with SS-316L was approximately 60.8% lower (3.85 vs. 9.83 arbitrary units of fluence/source; see Table 3) than with Al-6061-T6. Additionally, inelastic scattering with iron nuclei in SS-316L may contribute to moderating fast neutrons, thereby influencing the shape of the resulting spectrum.

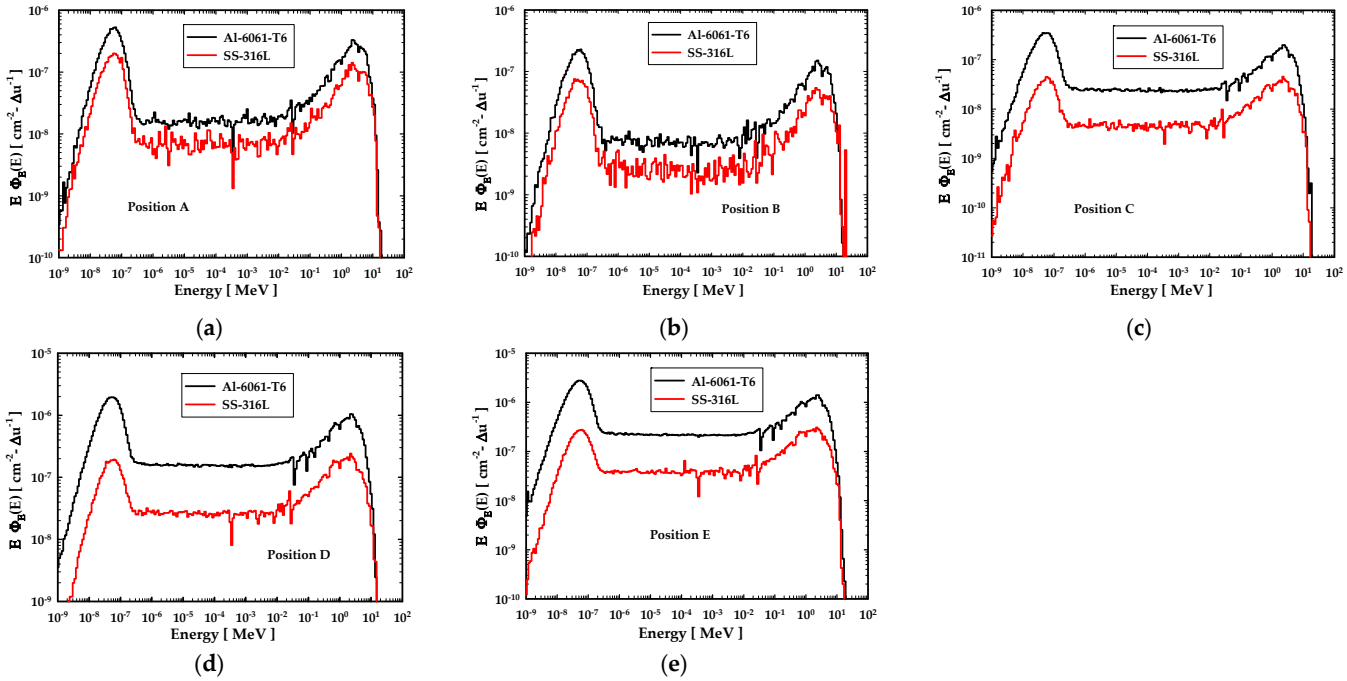


Figure 3. Comparisons of neutron spectra at positions A, B, C, D, and E in the NC-9000 reactor with Al-6061-T6 and SS-316L tubes: (**a**) Lateral near-core, (**b**) lateral elevated, (**c**) top experimental zone, (**d**) upper instructional area, and (**e**) reactor top center above the ^{239}PuBe source.

Table 3. Integrated neutron fluences (neutrons·cm^{-2}·source^{-1}) by energy ranges (thermal, epithermal, and fast) and their corresponding percentage uncertainties for the housing tube materials Al-6061-T6 (Al) and SS-316L (SS) at the five measurement positions (A–E) within the NC-9000 reactor.

Position	Thermal		Uncertainty (%)		Epithermal		Uncertainty (%)		Fast		Uncertainty (%)	
	Al	SS	Al	SS	Al	SS	Al	SS	Al	SS	Al	SS
A	9.83	3.85	1.13	2.18	11.59	4.61	1.04	2.01	19.84	8.10	0.77	1.46
B	4.39	1.48	1.56	3.17	5.17	1.76	1.43	2.94	8.85	3.14	1.04	2.14
C	7.46	0.88	0.61	1.94	10.11	1.38	0.51	1.49	15.81	2.70	0.4	1.02
D	42.64	4.17	0.43	1.11	59.81	7.01	0.36	0.86	92.31	14.59	0.29	0.62
E	59.69	5.90	0.34	0.86	83.80	10.08	0.29	0.79	127.55	20.36	0.25	0.56

At position B (Figure 3b), the total neutron fluence is lower than that observed at position A for both materials (Table 3). The trend of a generally lower neutron fluence with the SS-316L tube than Al-6061-T6 persists, consistent with stainless-steel intrinsic absorption properties. While Figure 3b shows that SS-316L maintains a lower spectral intensity, especially in the thermal region, the relative magnitude of the fluence reduction

due to the housing tube material (Al/SS factor) is comparable to or even slightly greater at position B than at A for specific energy ranges (see Table 3). For example, the thermal neutron Al/SS reduction factor is approximately 2.55 at position A and 2.97 at position B.

At position C (Figure 3c), neutron fluences remain generally low, comparable to or even higher than those at position B for Al-6061-T6 in some energy ranges (Table 3). SS-316L continues to exhibit a significantly lower spectral intensity than Al-6061-T6 across all energy ranges, with the reduction being particularly pronounced for thermal neutrons, a direct result of its higher neutron absorption cross-section. The Al/SS reduction factor for thermal neutrons at position C ($7.46/0.88 \approx 8.48$) is considerably higher than at positions A ($\approx$2.55) and B ($\approx$2.97), indicating a more pronounced attenuation effect from SS-316L at this position compared to A and B.

At position D (Figure 3d), substantially higher neutron fluences were recorded across all energy ranges for both materials evaluated (Al-6061-T6 and SS-316L) compared to positions A, B, and C, as detailed in Table 3. For instance, the thermal fluence with Al-6061-T6 at position D reaches a value of 42.64, which is approximately 4 to 9 times greater than that observed at positions A (9.83), B (4.39), or C (7.46). This high neutron intensity, illustrated in Figure 3d, even exceeds that of positions A and B. This suggests that although the distance from the source generally leads to the attenuation of neutron fluence at position D, this effect is counteracted by significant scattering and moderation phenomena near the core, resulting in a recovery and increase of the total fluence. Despite the overall fluence increase at position D, the attenuation introduced by the SS-316L material remains pronounced due to its intrinsic composition; the Al/SS reduction factor for thermal neutrons is approximately 10.2 and around 8.5 for epithermal neutrons. Consequently, the low energy intensity for SS-316L at this position remains comparatively lower than that for Al-6061-T6.

At position E (Figure 3e), which is located directly above the ^{239}PuBe source, the highest neutron fluences of this study were recorded (Table 3). Regarding fast neutrons, the fluence reduction factor when switching from Al-6061-T6 to SS-316L is approximately 6.26 (127.55 units with Al-6061-T6 vs. 20.36 units with SS-316L). This factor is comparable to those observed at positions D ($\approx$6.33) and C ($\approx$5.85) and even higher than those at positions A ($\approx$2.45) and B ($\approx$2.82). Therefore, SS-316L continues to significantly attenuate the magnitude of fast neutron fluence at position E compared to Al-6061-T6, which is consistent with the expected neutron interactions for this material.

Finally, the sharp local peaks observed in the fast neutron spectrum for SS-316L can be attributed to inelastic scattering events primarily involving Fe, Cr, and Ni, which constitute the majority of the alloy composition. According to the defined material card, SS-316L contains approximately 65% Fe, 17% Cr, and 12% Ni by weight. These elements exhibit significant inelastic cross-sections in the 0.5–3 MeV range, leading to localized energy redistribution [28]. Inelastic interactions with Mo and Mn also contribute to the overall effect. The relatively high density of SS-316L (8.00 g/cm^3) further increases the probability of such interactions, making the spectral peaks more pronounced in the fast neutron region compared to Al-6061-T6.

Table 4 presents the Al/SS reduction factors for each energy range (thermal, epithermal, and fast), along with the corresponding relative percentages and the total neutron fluence values for each position, expressed in arbitrary units per source particle. This provides a complete overview of the spectral behavior under both cladding materials.

Table 4. Comparison of neutron fluence reduction factors, spectral distribution (%), and total fluence (neutrons·cm^{-2}·source^{-1}) for Al-6061-T6 and SS-316L at key positions.

Position	Al/SS			% Al/SS			Al/SS
	Thermal	Epithermal	Fast	Thermal	Epithermal	Fast	Total Fluence
A	2.5	2.5	2.5	24/23	28/29	48/47	41.26/16.56
B	3.0	2.9	2.8	25/26	28/28	48/46	18.41/6.38
C	8.5	7.3	5.9	22/18	30/28	47/54	33.38/4.96
D	10.2	8.5	6.3	22/16	31/27	47/57	194.76/25.77
E	10.1	8.3	6.3	22/16	31/28	47/56	271.04/36.34

In summary, both the qualitative analysis of neutron spectra (Figure 3) and the quantitative data on integrated fluences (Table 3) consistently demonstrate that the use of SS-316L as a housing tube in replacement of Al-6061-T6 results in a substantial reduction in neutron fluence across all positions and energy ranges. This decrease is due to the higher neutron absorption cross-section and lower moderation capability of SS-316L. Although this reduction in fluence is a significant consideration for applications needing high neutron intensity, the proposal to evaluate SS-316L considers a wider range of properties to enhance reactor safety and longevity. SS-316L stainless steel presents substantial potential benefits in terms of structural strength, corrosion resistance, and high-temperature performance when compared to Al-6061-T6. These factors are critical for the long-term integrity and operational safety of the reactor. This study quantifies the neutronic impact of this potential substitution, revealing a reduction in fluence and a significant influence on spectral shape, with consistently higher average energies observed for SS-316L. These findings are vital: they enable an informed evaluation of the trade-offs between neutronic performance for experimentation and the essential improvements in robustness, safety, and longevity that SS-316L could provide. This comprehensive characterization is essential for advancing toward research reactors with globally optimized material performance.

In support of these findings, Table 4 offers a synthesized overview of the Al/SS reduction factors by energy range and detector position, along with relative spectral contributions and total neutron fluence. This tabulated comparison not only reinforces the observed attenuation trends but also provides a valuable framework for evaluating how material selection affects the spectral quality and intensity of the neutron field across various operational zones within the reactor.

The analysis of the integrated neutron fluences by energy ranges (thermal, epithermal, and fast), presented in Table 3, quantifies the differences in magnitude and energy distribution at positions A–E as a function of the housing tube material. Replacing Al-6061-T6 with SS-316L results in a reduction in fluence across all energy ranges and positions. The magnitude of this attenuation (expressed as the Al/SS reduction factor) is notably greater at positions D and E (total factors of approximately 7.5) compared to positions A and B (total factors of approximately 2.5–2.9), with position C falling in between (total factor of approximately 5.9). This suggests that the relative impact of SS-316L is more pronounced in regions of higher neutron fluence intensity (D and E), predominantly due to its higher neutron absorption capacity [29,30].

For thermal neutron fluence ($E < 0.1$ eV, Table 3), replacing Al-6061-T6 with SS-316L results in a marked decrease. This reduction is particularly severe at positions D and E, where thermal fluence decreases by approximately 10.2 (from 42.64 to 4.17 units at D) and approximately 10.1 (from 59.69 to 5.90 units at E), representing approximately 90% of attenuation in both cases. The reduction factors are lower at positions A and B (≈2.55 and ≈2.97,

respectively). Interestingly, the thermal neutron reduction factor at position C is also high (≈8.48), closer to the values observed at D and E than at A and B. These data confirm that SS-316L has a substantial impact on the thermal neutron population, consistent with the absorption cross-sections of its components, with a particularly pronounced influence in positions C, D, and E [31,32].

Similarly, the epithermal neutron fluence (0.1 eV < E < 100 keV, Table 3) is substantially reduced with the SS-316L tube. At position D, the Al/SS reduction factor is approximately 8.53 (from 59.81 to 7.01 units), and at position E, it is approximately 8.31 (from 83.80 to 10.08 units), corresponding to approximately 88% attenuation in both cases. At positions A and B, the reduction factors are lower (≈2.51 and ≈2.94, respectively), while at position C, the factor is higher (≈7.33). This significant interaction of SS-316L with epithermal neutrons can be partly attributed to absorption resonance phenomena in the steel components within this energy range, which clearly distinguish it from aluminum [33,34].

Fast neutron fluence (E > 100 keV, Table 3) also decreases with the SS-316L tube, although the magnitude of this reduction is generally smaller than that observed for thermal and epithermal neutrons. Specifically, at the high-fluence positions D and E, the Al/SS reduction factors for fast neutrons are approximately 6.33 and approximately 6.26, respectively. These values are lower than the reduction factors observed for thermal neutrons (≈10) and epithermal neutrons (8.3–8.5) at the same positions. This behavior suggests that, although SS-316L remains an effective attenuator of fast neutrons compared to Al-6061-T6, due to interactions such as inelastic scattering, its relative impact is less pronounced in the fast energy range than in the lower energy ranges, possibly due to differences in the cross-sections of the dominant reactions at these energies [35,36].

The observed variations in neutron fluence magnitude and energy distribution provide critical data for neutronics characterization of the reactor. The overall fluence reduction with SS-316L would directly impact reaction rates within the fuel (if applicable to the reactor design) [37,38], as well as the activation of surrounding structural or experimental materials [39,40]. Moreover, altering the energy spectrum would affect the planning and efficiency of experiments that depend on specific neutron energy ranges, such as neutron activation analysis or scattering studies [41]. These factors must be carefully addressed and planned for when considering material substitution, weighing them against the durability and safety benefits that motivate the evaluation of SS-316L.

The significantly higher neutron absorption by SS-316L, especially in the thermal and epithermal ranges, is primarily attributed to the presence of elements such as iron, chromium, and nickel in its composition, which have substantially higher neutron capture cross-sections than aluminum [42,43]. A detailed analysis based on microscopic cross-sections and the elemental composition of both materials would enable a more accurate modeling of the underlying mechanisms responsible for the observed differences [44,45].

In conclusion, the Monte Carlo simulation results indicate that replacing the Al-6061-T6 housing tube with SS-316L in the NC-9000 subcritical nuclear reactor significantly attenuates neutron fluence across all energy ranges and measurement positions analyzed. This change in both the magnitude and energy spectrum of the neutron fluence is undoubtedly a key factor when assessing the viability of SS-316L. However, the relevance of this investigation lies in the need to explore alternative materials, such as SS-316L, which can provide substantial and necessary improvements in other critical aspects, including structural integrity, corrosion resistance, or extended reactor lifetime, which are not captured solely by neutronic analysis. The implications of reduced neutron fluence will affect specific research and educational applications. Still, this study provides the quantitative data needed to weigh those effects against the crucial benefits to long-term operability and inherent safety offered by SS-316L. Moreover, the detailed characterization of the modified

radiation field and its impact on dosimetry, as analyzed in subsequent sections, is essential for a comprehensive evaluation and for identifying operational or experimental scenarios where the SS-316L profile may prove advantageous or acceptable within the context of a more robust and secure overall reactor design.

3.3. Neutron Dosimetry

The analysis of ambient neutron equivalent dose, $H^*(10)_n$ and H^*_n, at the five evaluated positions (A–E) within the NC-9000 reactor reveals a significant and highly favorable dependence on the core housing tube material, with clear advantages for SS-316L (Table 5). Using both the ICRP 74 and ICRU 95 dosimetric conversion coefficients [21,22,46,47], it is consistently observed that the SS-316L tube results in substantially lower neutron doses compared to Al-6061-T6. These international standards are justified by their broad recognition and the rigorous methodology underlying their development [48,49].

Table 5. The mean neutron energy (E_{mean}) and ambient neutron equivalent dose rate were calculated using ($H^*(10)_n$) ICRP 74 and (H^*_n) ICRU 95 coefficients for the housing tube materials Al-6061-T6 (Al) and SS-316L (SS) at the evaluated positions (A–E).

Position	E_{mean} [MeV]		$H^*(10)_n$ ICRP74 [μSv/h]		Uncertainty (%)		H^*_n ICRU95 [μSv/h]		Uncertainty (%)	
	Al	SS	Al	SS	Al	SS	Al	SS	Al	SS
A	1.14	1.25	10.98	4.66	0.98	1.81	10.20	4.36	1.02	1.88
B	1.16	1.39	4.89	1.86	1.19	2.87	4.57	1.75	1.23	2.89
C	0.73	1.01	7.02	1.59	0.45	1.16	6.10	1.38	0.47	1.21
D	0.65	0.97	39.27	8.92	0.29	0.76	33.32	7.59	0.30	0.87
E	0.61	0.92	52.67	12.07	0.27	0.68	44.35	10.21	0.28	0.77

From the perspective of radiological protection, one of the key arguments supporting the evaluation of SS-316L is reinforced by the dosimetric results. Quantitatively, using SS-316L as a housing tube material instead of Al-6061-T6 significantly reduces the ambient equivalent dose (calculated using ICRP 74 coefficients). This reduction ranges from a factor of approximately 2.3 at position A (from 10.98 μSv/h to 4.66 μSv/h) to an impressive factor of about 4.4 at position E (from 52.67 μSv/h to 12.07 μSv/h), This demonstrates SS-316L's capacity to enhance radiological safety, in complete alignment with the principle of keeping doses As Low As Reasonably Achievable (ALARA). Consequently, this material substitution results in a significant reduction in neutron exposure. Specifically, attenuation reaches approximately 77% at positions C (from 7.02 to 1.59 μSv/h), D (from 39.27 to 8.92 μSv/h), and E (from 52.67 to 12.07 μSv/h). In contrast, the attenuation at positions B (from 4.89 to 1.86 μSv/h) and A is 62% and 57%, respectively. The robustness of these findings is further supported by the agreement with the results obtained using ICRU 95 coefficients (Table 5), indicating a consistent and reliable assessment of neutron dose regardless of the coefficient set employed [50,51].

The mean neutron energy (E_{mean}) also varies according to the housing tube material, as shown in Table 5: neutrons exhibit slightly higher average energies when the core is clad with SS-316L. This finding suggests that SS-316L has a lower neutron moderation capability compared to Al-6061-T6, an interpretation consistent with the differences in neutron spectra reported by [52]. This reduced moderation efficiency, along with the higher neutron absorption cross-section of SS-316L (due to elements like Fe, Cr, and Ni [52,53]), results in reduced thermal and epithermal neutron fluences in the regions surrounding the

reactor, which directly translates into the lower ambient equivalent doses observed with this material. This marked reduction in ambient neutron dose represents a significant operational and safety advantage, potentially facilitating compliance with dose limits, reducing shielding requirements, or improving working conditions for personnel near the reactor. This finding alone constitutes a compelling argument that justifies the evaluation and consideration of SS-316L, even in light of the reduced neutron fluence intensity available for experimentation.

Although Table 5 focuses on neutron dosimetry, the impact of the housing tube material on gamma radiation dose is also a critical consideration for a comprehensive safety evaluation. While the experimental quantification of gamma dose was not part of this study, the following mechanisms explain how the housing tube material could influence it:

a. Neutron activation of SS-316L: The significantly higher neutron capture cross-sections of the constituent elements of SS-316L (such as Fe, Cr, and Ni) compared to those in Al-6061-T6 [54] would result in an increased production of gamma-emitting radioisotopes within the steel tube itself [55].
b. Modulation of secondary gamma production: SS-316L modulates secondary gamma production by attenuating and modifying the neutron spectrum in a way that differs from Al-6061-T6 [56], which would influence the production of secondary gamma rays in other reactor components. Specifically, increased neutron absorption within the SS-316L tube could reduce secondary gamma production in adjacent moderators or coolants (due to the lower incident neutron fluence). In contrast, the activation of the steel tube itself would generate an additional source of gamma emission simultaneously.
c. These findings are consistent with previous studies [5], which have reported a correlation between materials with high neutron absorption capacity and reduced gamma dose levels near activated radiation sources. An essential next step involves a detailed quantitative evaluation of the gamma dose contribution, including spectral analysis and identifying relevant activated radionuclides. The possibility, suggested by studies such as [5], that SS-316L may contribute to a reduction in external gamma dose due to the overall alteration of the radiation field, despite its activation, was one of the motivating hypotheses behind the present material evaluation. Confirming such an effect would significantly strengthen the suitability of SS-316L for applications where minimizing the total dose (neutron and gamma) is the primary goal, complementing its structural advantages and justifying its consideration despite the reduction in neutron fluence available for experimentation.

3.4. Gamma-Ray Spectra

The comparative analysis of gamma-ray spectra at positions A, B, C, D, and E (illustrated in Figure 4, which details the gamma spectral distribution at each point) reveals a clear trend when contrasting the Al-6061-T6 and SS-316L tubes. At these locations, the gamma spectrum associated with the Al-6061-T6 tube generally exhibits higher magnitudes across most energy ranges, with the notable exception of the 6 to 10 MeV interval, as observed in Figure 4a–e. This behavior aligns with the lower gamma attenuation capability of Al-6061-T6, attributable to its lower density and effective atomic number compared to SS-316L [57,58].

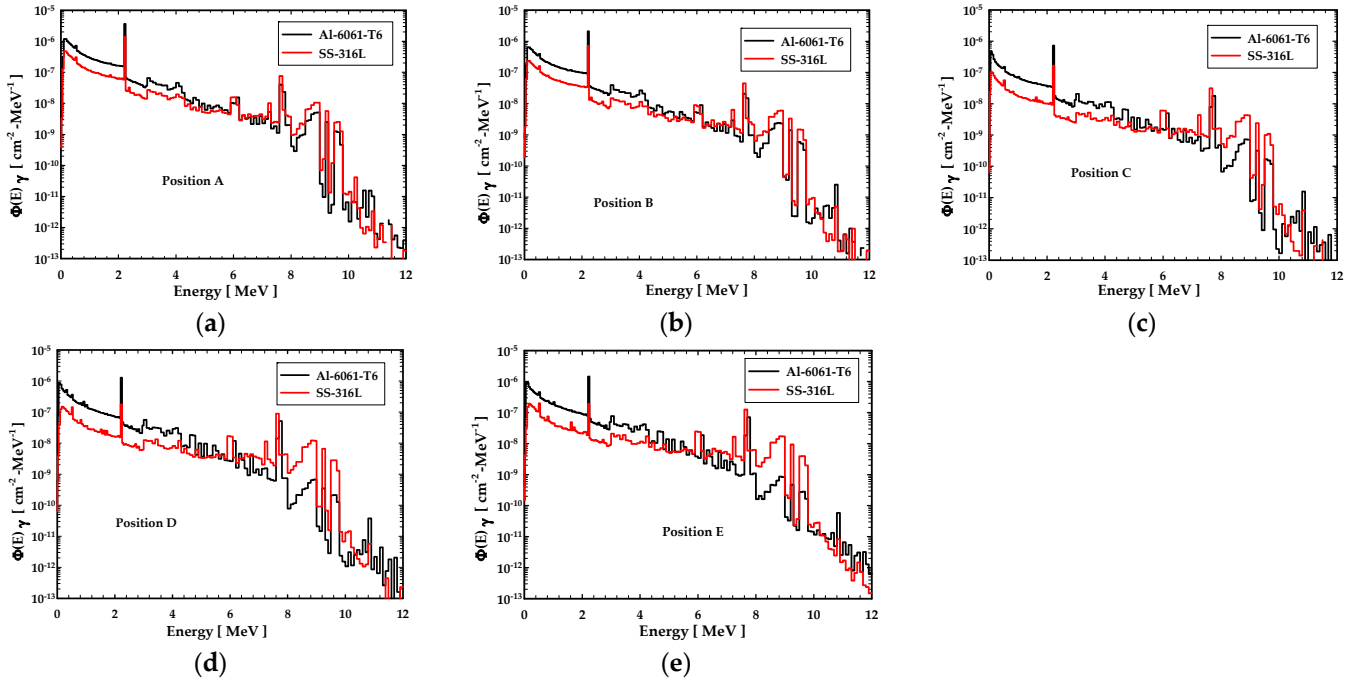


Figure 4. Comparison of gamma-ray spectra at the different detector positions in the NC-9000 reactor, with Al-6061-T6 and SS-316L tubes: (**a**) Lateral near-core, (**b**) lateral elevated, (**c**) top experimental zone, (**d**) upper instructional area, and (**e**) reactor top center above the ^{239}PuBe source.

However, it is essential to emphasize that while SS-316L induces more pronounced attenuation, the overall shape and energy distribution of the gamma spectra remain remarkably like those obtained with Al-6061-T6 (except in the mentioned energy range), where a relative increase is observed in Figure 4c–e. This preservation of spectral characteristics is a significant finding, as it suggests that replacing Al-6061-T6 with SS-316L would not substantially alter the nature of gamma radiation present during experiments, thus maintaining the validity of current spectroscopic and dosimetric measurements. This initial result already suggests that SS-316L is a promising alternative, as it does not significantly alter the gamma spectrum.

In position E (Figure 4e), where the radiation source is directly adjacent to the bottom of the detector, the simulation reveals an interesting behavior: SS-316L reaches slightly higher spectral intensity levels than Al-6061-T6 in specific energy ranges. This result highlights the complexity of radiation–material interactions in specific geometries. It suggests that SS-316L may experience an increase in gamma-ray fluence in the 6–10 MeV energy range under direct exposure to the source. Despite this peculiarity under direct exposure, SS-316L still demonstrates a performance comparable to that of Al-6061-T6.

3.5. Gamma-Ray Dosimetry Spectra

The quantitative analysis of gamma-ray equivalent doses at the five points of interest (Table 6) complements the spectral evaluation. The results consistently show that SS-316L results in significantly lower doses at positions A, B, C, D, and E compared to Al-6061-T6. Specifically, at position A, a reduction of approximately half the magnitude in the equivalent dose $(H^*(10)_\gamma$ according to ICRP 74, and as H^*_γ under the updated definition from ICRU Report 95) is observed when SS-316L is used as a housing tube [59–61]. This marked difference highlights the superior gamma attenuation capacity of SS-316L, which directly translates into a substantial improvement in radiological protection around the reactor, further consolidating its potential as an excellent alternative.

Table 6. Gamma dose rates for Al-6061-T6 and SS-316L.

Position	E_{mean} [MeV]		$H^*(10)_\gamma$ ICRP74 [μSv/h]		Uncertainty [%]		H^*_γ ICRU95 [μSv/h]		Uncertainty [%]	
	Al	**SS**	**Al**	**SS**	**Al**	**SS**	**Al**	**SS**	**Al**	**SS**
A	1.26	1.40	4.61	2.01	0.42	0.54	3.99	1.74	0.42	0.54
B	1.27	1.46	2.66	1.09	0.56	0.74	2.31	0.94	0.56	0.74
C	1.17	1.55	1.05	0.36	0.56	0.67	0.91	0.31	0.56	0.67
D	1.19	1.80	2.24	0.74	0.41	1.20	1.94	0.64	0.41	1.21
E	1.23	1.93	2.80	0.99	0.41	0.65	2.43	0.86	0.41	0.65

Overall, the Monte Carlo simulation results provide strong evidence for considering SS-316L as a viable and preferable alternative to the current housing tube material for the NC-9000 reactor. While Al-6061-T6 exhibits slightly lower gamma attenuation at peripheral positions in specific energy ranges, SS-316L consistently demonstrates the superior capability to reduce equivalent doses, which is crucial for radiological safety and the longevity of reactor components.

Although the use of SS-316L cladding results in a slightly higher mean gamma photon energy, the ambient gamma equivalent dose H*(10) is consistently lower at all evaluated positions compared to the Al-6061-T6 case. This outcome is due to the higher density and effective atomic number of SS-316L, which enhances its attenuation capability for gamma photons. Therefore, from a radiation protection standpoint, SS-316L does not pose an increased hazard; rather, it contributes to improved radiological safety in the reactor environment.

The observed similarity in gamma spectrum shapes confirms that adopting SS-316L would maintain experimental functionality for gamma spectroscopy without significant alteration [62,63]. Therefore, SS-316L is a robust alternative that prioritizes safety without sacrificing research capability.

The Monte Carlo simulation demonstrates the potential of SS-316L as a suitable replacement for Al-6061-T6 as a housing tube material in the NC-9000 reactor. By offering greater corrosion resistance [64] without causing drastic changes in gamma-ray spectra, this material presents a viable alternative for improving the reactor's durability and safety without affecting its fundamental value for research and education. These results underscore the need for further experimental investigation into the properties and performance of SS-316L, specifically within the operational context of the NC-9000 reactor, which could further confirm its suitability as a superior material for housing tubes [65,66].

The comprehensive evaluation of neutron and gamma doses is essential to ensure the radiological safety of operational personnel and the surrounding environment. The values obtained must be rigorously compared with occupational dose limits established by international [67] and national [68] regulations. The apparent reduction in gamma dose with SS-316L, as shown in Table 6, further underscores its advantage in terms of radiological safety.

4. Summary of Findings, Implications, and Research Outlook

Based on detailed simulations using the MCNP5 code, this study conducted a comprehensive comparative evaluation of the impact of replacing the Al-6061-T6 used in the tubes hosting the fuel slugs with SS-316L to address the corrosion problems. The impact

was evaluated in the k_{eff}, neutron, and gamma-ray spectra and doses outside the NC-9000 subcritical nuclear reactor.

The results obtained for the effective multiplication factor ($k_{eff} < 1$) confirmed the inherently subcritical condition of the reactor for both housing tube configurations, ensuring an intrinsic margin of operational safety. The observed decrease in k_{eff} with SS-316L, attributed to its higher neutron absorption, further reinforces this passive safety characteristic.

Neutron spectral analysis at the positions of interest (A–E) revealed significant fluence attenuation across the entire energy range when using SS-316L, with the effect being most pronounced for thermal and epithermal energies, particularly near the core. This phenomenon is due to the higher neutron absorption cross-section of SS-316L at these energies, influenced by elements such as Fe, Cr, and Ni [42,43]. Additionally, the lower neutron moderation observed with SS-316L, evidenced by slightly higher average neutron energies (Table 5), contributes to spectral modification with direct implications for neutron dosimetry. The reduced availability of thermal and epithermal neutrons with SS-316L could impact the planning and outcomes of neutron activation experiments and neutron scattering studies [41], requiring careful consideration in experimental design and data interpretation.

Regarding gamma radiation, SS-316L demonstrated greater attenuation effectiveness at peripheral positions (A–E), except in the 6 to 10 MeV energy range, representing a significant advantage for radiological protection (Table 5). The similarity in the overall shape of the gamma spectra for both housing tube materials suggests that the material change would not substantially alter the quality of gamma radiation generated in the reactor, thus preserving the validity of spectroscopic measurements [62,63]. This gamma attenuation capability of SS-316L underscores its potential to enhance reactor environmental safety.

The neutron dosimetric results showed a substantial reduction in ambient equivalent dose when using SS-316L as a housing tube, with notable decreases of up to approximately 77% at key locations (Table 5). The consistency between calculations based on the ICRP 74 and ICRU 95 dosimetric conversion coefficients reinforces the robustness and reliability of these findings, highlighting a clear advantage of SS-316L in protecting operational personnel and the surrounding environment.

However, the potentially higher gamma spectral intensity in the 6 to 10 MeV range at positions C, D, and E for housing tubes made of SS-316L calls for a thorough experimental investigation to confirm this finding and understand its dosimetric implications. Future experimental studies should focus on the detailed measurement of gamma-ray spectra at these specific positions using high-resolution detectors and quantifying the resulting gamma doses to validate the simulation predictions.

The proposed substitution of Al-6061-T6 tubes with SS-316L in the NC-9000 reactor significantly enhances radiological safety and operational longevity. The superior gamma attenuation provided by SS-316L leads to a notable reduction in ambient neutron dose, creating a safer environment for personnel. Furthermore, its superior corrosion resistance [64] will likely prolong the operational lifetime of the reactor. While the material change may decrease thermal and epithermal neutron fluence, this potential impact can be carefully managed through considerations in the design of reactor physics, neutron physics, and health physics experiments. The balance of these factors strongly supports the viability and benefits of adopting SS-316L as the housing tube material, offering tangible improvements in safety and durability for the NC-9000 reactor.

Based on the above, this study provides a solid foundation for considering SS-316L as a viable and potentially advantageous alternative to Al-6061-T6 in the NC-9000 reactor, particularly concerning radiological safety. Future experimental and analytical investigations will be essential to verify these findings and comprehensively evaluate the effects

of this material substitution on the experimental performance and long-term operation of the reactor.

5. Conclusions

The comparative MCNP5 simulation of Al-6061-T6 and SS-316L materials for the tubes hosting fuel slugs in the subcritical nuclear reactor, Nuclear Chicago model 9000, confirmed subcriticality in both cases while revealing distinct impacts on radiation behavior. Al-6061-T6 was favored by its higher neutron fluence, whereas SS-316L effectively attenuated peripheral gamma radiation and significantly reduced the neutron dose, thereby enhancing radiological safety. The spectral similarity in gamma rays suggests that there is no significant alteration for spectroscopic experiments. The superior corrosion resistance of SS-316L implies greater potential durability. Despite a reduction in neutron fluence, the improvements in radiological safety and structural longevity make SS-316L a promising alternative. An experimental evaluation of SS-316L activation and gamma dose near the fuel is recommended to confirm its long-term viability.

Author Contributions: Conceptualization, D.M.-C. and H.R.V.-C.; methodology, A.B.-R. and T.G.S.-B.; software, H.R.V.-C. and R.L.-C.; validation, D.M.-C. and B.G.R.-M.; formal analysis, A.B.-R. and T.G.S.-B.; investigation, D.M.-C. and R.L.-C.; resources, D.M.-C. and B.G.R.-M.; data curation, D.M.-C. and B.G.R.-M.; writing—original draft preparation, D.M.-C.; writing—review and editing, D.M.-C., R.L.-C. and B.G.R.-M.; supervision, H.R.V.-C., A.B.-R. and T.G.S.-B. All authors have read and agreed to the published version of the manuscript.

Funding: The National Institute for Nuclear Research partially funded this study through the DI-02A project.

Data Availability Statement: Data is contained within the article.

Conflicts of Interest: The authors declare no conflicts of interest.

Abbreviations

The following abbreviations are used in this manuscript:

6061-T6	A 6000 series aluminum alloy that has been heat-treated
Al	Aluminum
Be	Beryllium element
Bq	Becquerel is the standard international unit of measurement for radioactivity
ICRP	International Commission on Radiological Protection
ICRU	International Commission on Radiation Units and Measurements
MCNP	Monte Carlo N-Particle
NC-9000	Nuclear Chicago model 9000
Pu	Plutonium element
SS-316L	316L stainless steel (low carbon, highly corrosion-resistant).
UAZ	Autonomous University of Zacatecas
Φ	Neutron fluence

References

1. Jarrah, I.; Malkawi, S.; Radaideh, M.S.; Aldebie, F.; El-Mustafah, M. Experimental validation of the neutronic parameters in the Jordan subcritical assembly. *Prog. Nucl. Energy* **2018**, *108*, 71–80. [CrossRef]
2. Ni, Z.; Xie, J.; Wasaye, M.A.; Zhang, E.; Yu, T. Effect of higher-order harmonics on the steady-state neutron flux in accelerator-driven subcritical reactors. *Int. J. Energy Res.* **2023**, *2023*, 4114886. [CrossRef]
3. Yan, S.; Zhou, L.; Song, L.; Guo, H.; Wu, J.; Luo, R.; Zhao, F. Collaborative control and intelligent optimization of a lead–bismuth cooled reactor based on a modified PSO method. *Energies* **2025**, *18*, 567. [CrossRef]
4. Papastefanou, C. Measurement of neutron flux and albedo of water for thermal neutrons with foils of indium in a subcritical nuclear reactor. *J. Radioanal. Nucl. Chem.* **2004**, *261*, 671–678. [CrossRef]

5. Vega-Carrillo, H.R.; Garcia-Reyna, M.G.; Marquez-Mata, C.A.; Vazquez-Bañuelos, J.; Campillo-Rivera, G.E.; Bedenko, S.V. Effect of changing the neutron moderator in a thermal subcritical nuclear reactor. *Appl. Radiat. Isot.* **2022**, *188*, 110395. [CrossRef]
6. Tilloy, A. Arbitrarily large neutron amplification in subcritical nuclear reactors. *Phys. Rev. Appl.* **2021**, *16*, 014059. [CrossRef]
7. Malkawi, S.; Sweidan, F.; Khalifeh, H. Reactivity determination in a subcritical reactor: Computational, analytical and experimental methods. *Ann. Nucl. Energy* **2021**, *161*, 108432. [CrossRef]
8. Deng, N.; Xie, C.; Hou, C.; Li, Z.; Xie, J.; Yu, T. The influence mechanism of neutron kinetics of the accelerator-driven subcritical reactor based on the fast/thermal neutron spectra by Monte Carlo homogenization method. *Energies* **2023**, *16*, 3545. [CrossRef]
9. Xiong, H.-H.; Zeng, Q.-S.; Han, Y.-C.; Ren, L.; Baidoo, I.K.; Chen, N.; Zeng, Z.-K.; Wang, X.-Y. Neutronics analysis of a subcritical blanket system driven by a gas dynamic trap-based fusion neutron source for 99Mo production. *Nucl. Sci. Tech.* **2023**, *34*, 49. [CrossRef]
10. Janczyszyn, J.; Domańska, G.; Oettingen, M. Simulation of the measured reactivity distributions in the subcritical MYRRHA reactor. *Energies* **2024**, *17*, 2565. [CrossRef]
11. Du, W.; Zhao, X. Nuclear reaction modeling of neutron induced reactions on 208Pb. *Eur. Phys. J. A* **2025**, *61*, 52. [CrossRef]
12. Yu, X.; Zhang, G.; Zhang, Z.; Wang, Y. Research on corrosion resistance of anodized and sealed 6061 aluminum alloy in 3.5% sodium chloride solution. *Int. J. Electrochem. Sci.* **2023**, *18*, 100092. [CrossRef]
13. Vega-Carrillo, H.R.; Aguilar-Dominguez, A.L.; Bedenko, S.V.; García-Fernandez, G.F. Computational spectrometry and dosimetry of neutrons and γ rays outside a subcritical nuclear reactor with water and polyethylene moderators. *Radiat. Phys. Chem.* **2023**, *204*, 110719. [CrossRef]
14. De la Torre-Aguilar, F.; Davila-Rangel, J.I.; Robles-Luna, A.; Mireles-García, F.; Ríos-Martínez, C.; Pinedo-Vega, J.L. History and current status of the subcritical nuclear reactor of the Universidad Autónoma de Zacatecas. In Proceedings of the 34th Annual Congress of the Mexican Nuclear Society: Small Modular Reactors, a New Perspective for Nuclear Energy in Mexico, La Paz, Mexico, 27–30 August 2023.
15. Sganzerla, W.G.; Zabot, G.L.; Torres-Mayanga, P.C.; Buller, L.S.; Mussatto, S.I.; Forster-Carneiro, T. Techno-economic assessment of subcritical water hydrolysis process for sugars production from brewer's spent grains. *Ind. Crops Prod.* **2021**, *171*, 113836. [CrossRef]
16. Sganzerla, W.G.; Moreira, B.P.; Lachos-Perez, D.; Zabot, G.L.; Nochi Castro, L.E.; Forster-Carneiro, T.; Rostagno, M.A. Techno-economic analysis of amino acids production with subcritical water technology. *J. Supercrit. Fluids* **2025**, *222*, 106595. [CrossRef]
17. Vega-Carrillo, H.R.; Villagrana-Muñoz, L.E.; Rivera-Perez, E.; de Leon-Martinez, H.A.; Soto-Bernal, T.G.; Hernández-Davila, V.M. Concrete enclosure for shielding a neutron source. *Appl. Radiat. Isot.* **2013**, *79*, 37–41. [CrossRef]
18. Brown, F.B. MCNP5 development, verification, and performance. In Proceedings of the International Conference on Supercomputing in Nuclear Applications (SNA 2003), Paris, France, 22–24 September 2003.
19. Sood, A.; Forster, R.A.; Archer, B.J.; Little, R.C. Neutronics calculation advances at Los Alamos: Manhattan Project to Monte Carlo. *Nucl. Technol.* **2021**, *207* (Suppl. S1), S100–S133. [CrossRef]
20. National Council on Radiation Protection and Measurements (NCRP). *Calibration of Survey Instruments Used in Radiation Protection for the Assessment of Ionizing Radiation Fields and Radioactive Surface Contamination*; NCRP Report No. 112; NCRP: Bethesda, MD, USA, 1991.
21. International Commission on Radiological Protection (ICRP). *Conversion Coefficients for Use in Radiological Protection Against External Radiation*; ICRP Publication 74; Pergamon Press: Oxford, UK, 1997.
22. International Commission on Radiation Units and Measurements (ICRU). *Operational Quantities for External Radiation Exposure*; ICRU Report 95; ICRU: Bethesda, MD, USA, 2020.
23. Oettingen, M.; Döderlein, C.; D'Agata, E.; Tucek, K.; Cetnar, J. Comparison of MCB and FISPACT burn-up performances using the HELIOS experiment technical specifications. *Nucl. Eng. Des.* **2012**, *242*, 399–412. [CrossRef]
24. Zinkle, S.J.; Was, G.S. Materials challenges in nuclear energy. *Acta Mater.* **2013**, *61*, 735–758. [CrossRef]
25. Ma, H.; Fan, P.; Qian, Q.; Zhang, Q.; Li, K.; Zhu, S.; Yuan, D. Nanoindentation test of ion-irradiated materials: Issues, modeling and challenges. *Materials* **2024**, *17*, 3286. [CrossRef]
26. El-Khayatt, A.M. Calculation of photon shielding properties for some neutron shielding materials. *Nucl. Sci. Tech.* **2017**, *28*, 69. [CrossRef]
27. Akkurt, I.; Boodaghi Malidarre, R. Gamma photon-neutron attenuation parameters of marble concrete by MCNPX code. *Radiat. Eff. Defects Solids* **2021**, *176*, 906–918. [CrossRef]
28. Duderstadt, J.J.; Hamilton, L.J. *Nuclear Reactor Analysis*; John Wiley & Sons: New York, NY, USA, 1976; Chapter 3; pp. 74–100.
29. Griffiths, M. Effect of neutron irradiation on the mechanical properties, swelling and creep of austenitic stainless steels. *Materials* **2021**, *14*, 2622. [CrossRef] [PubMed]
30. Ye, X.P.; Hu, J.B.; Gu, Y.Q.; Nan, X.L.; Li, X.M.; Duan, Z.W.; Ying, Y.Y.; Cai, L.C.; Liu, C.L. Effects of pre-stress on the mechanical properties and microstructure of neutron-irradiated high-purity aluminum. *J. Nucl. Mater.* **2023**, *573*, 154126. [CrossRef]

31. Yang, S.; Yao, Y.; Wang, H.; Huang, H. A comparative study of neutron shielding performance in Al-based composites reinforced with various boron-containing particles for radiotherapy: A Monte Carlo simulation. *Nanomaterials* **2024**, *14*, 1696. [CrossRef]
32. Donya, H.; Umer, M. Optimization of DD-110 neutron generator output for boron neutron capture therapy using Monte Carlo simulation. *Quantum Beam Sci.* **2025**, *9*, 12. [CrossRef]
33. Aziz, F.; Rivai, A.K.; Panitra, M.; Dani, M.; Suharno, B. Accident tolerant fuel cladding materials for light water reactors: Analysis of neutronic characteristics. *Int. J. Technol.* **2024**, *15*, 608–617. [CrossRef]
34. Hirsh, T.Y.; Leong, A.F.T.; Losko, A.S.; Wolfertz, A.; Savage, D.J.; Jäger, T.T.; Rakovan, J.; Wall, J.J.; Long, A.M.; Vogel, S.C. Energy-resolved neutron imaging and diffraction including grain orientation mapping using event camera technology. *Sci. Rep.* **2025**, *15*, 12901. [CrossRef]
35. Hamrashdi, H.A.; Cheneler, D.; Monk, S.D. A fast and portable imager for neutron and gamma emitting radionuclides. *Nucl. Instrum. Methods Phys. Res. Sect. A* **2020**, *953*, 163253. [CrossRef]
36. Košťál, M.; Losa, E.; Czakoj, T.; Schulc, M.; Šimon, J.; Juříček, V.; Rypar, V.; Ulmanová, J.; Trkov, A.; Capote, R. The effect of heavy reflector on neutronic parameters of core. *Ann. Nucl. Energy* **2022**, *168*, 108898. [CrossRef]
37. Mirvakili, S.M.; Gholamzadeh, Z.; Davari, A. Neutronic and thermo-hydraulic analysis of a modeled subcritical uranyl nitrate aqueous reactor driven by 30-MeV protons. *Ann. Nucl. Energy* **2016**, *97*, 171–178. [CrossRef]
38. Kolos, K.; Sobes, V.; Vogt, R.; Romano, C.E.; Smith, M.S.; Bernstein, L.A.; Brown, D.A.; Burkey, M.T.; Danon, Y.; Elsawi, M.A.; et al. Current nuclear data needs for applications. *Phys. Rev. Res.* **2022**, *4*, 021001. [CrossRef]
39. Wang, J.; Zhang, S.; Han, F.; Luo, Y.; Chen, J.; Hu, Z.-T.; Pan, Z.; Hu, M. Corrosion performance and mechanisms of tantalum coatings on 316 stainless-steel in subcritical aqueous solutions of NaCl and NaBr. *Corros. Sci.* **2024**, *231*, 112006. [CrossRef]
40. Guo, F.; Zhang, L.; Gu, L.; Jiang, W. Optimization design and deterministic analyses based on the multitype PD ratio fuel assemblies of small long life lead cooled fast reactor. *Nucl. Eng. Des.* **2024**, *428*, 113478. [CrossRef]
41. Poenitz, E.; Nolte, R.; Schmidt, D.; Chen, G. Study of the 15N(p,n)15O reaction as a monoenergetic neutron source for the measurement of differential scattering cross sections. *J. Instrum.* **2017**, *12*, P03016. [CrossRef]
42. Parker, S.F.; Baker, P.J.; McGreevy, R. A vision for the future of neutron scattering and muon spectroscopy in the 2050s. *ACS Phys. Chem. Au* **2024**, *4*, 439–452. [CrossRef]
43. Melo, J.P.C.; Chaves, L.V.G.; Silva, S.V.F.; Duarte, J.; Corrêa, K.M.S.; Oliveira, N.G.P.L.; Cassimiro, J.; Velasquez, C.E.; da Silva, C.A.M.; Pereira, C. Evaluation of different external neutron sources for a hybrid system based on the SEALER reactor. *Ann. Nucl. Energy* **2025**, *214*, 111234. [CrossRef]
44. Lucia, U.; Grisolia, G. Energy amplifier systems as sustainable nuclear reactors: An overview. *Sustainability* **2024**, *16*, 2743. [CrossRef]
45. Marques, R.V.A.; Velasquez, C.E.; Pereira, C. Neutronic evaluation for different external neutron sources in a small-subcritical fast reactor. *Nucl. Eng. Des.* **2024**, *417*, 112868. [CrossRef]
46. Pozzi, F.; Ferrarini, M.; Ferrulli, F.; Silari, M. Impact of the newly proposed ICRU/ICRP quantities on neutron calibration fields and extended range neutron rem-counters. *J. Radiol. Prot.* **2019**, *39*, 920–937. [CrossRef]
47. García-Fernandez, G.F.; Gallego, E.; Gómez-Ros, J.M.; Vega-Carrillo, H.R.; Guzmán-García, K.A.; Cevallos-Robalino, L.E.; García-Baonza, R.; Fuentes-Hernández, E. Benchmarking of stray neutron fields produced by synchrocyclotrons and synchrotrons in compact proton therapy centers (CPTC) using MCNP6 Monte Carlo code. *Appl. Radiat. Isot.* **2023**, *193*, 110645. [CrossRef] [PubMed]
48. Kim, M.C.; Kim, H.; Han, H.; Choi, Y.; Kim, S.; Lee, J.; Min, B.I.; Suh, K.; Kim, C.K. Calculation of dose conversion coefficients for radiation workers in various postures. *Radiat. Phys. Chem.* **2025**, *229*, 112413. [CrossRef]
49. Caridi, F.; Mottese, A.F.; Paladini, G.; Pistorino, L.; Gregorio, F.; Lanza, S.; Randazzo, G.; Marguccio, S.; Belvedere, A.; D'Agostino, M.; et al. Multivariate statistics, radioactivity and radiological hazard evaluation in marine sediments of selected areas from Sicily, Southern Italy. *J. Mar. Sci. Eng.* **2025**, *13*, 769. [CrossRef]
50. Asadov, S.M.; Mustafaeva, S.N.; Guseinov, D.T.; Kelbaliev, K.I. Dependence of the X-ray dosimetric parameters of $AgGaS_{2x}Se_{2-2x}$ single crystals on their composition. *Tech. Phys.* **2018**, *63*, 546–550. [CrossRef]
51. El Bakkali, J.; Doudouh, A.; El Bardouni, T.; Ghalbzouri, T.E.L.; Yerrou, R. Intercomparison of S-Factor values calculated in Zubal voxelized phantom for eleven radionuclides commonly used in targeted prostate cancer therapy. *Phys. Eng. Sci. Med.* **2022**, *45*, 1251–1256. [CrossRef]
52. Qi, Z.; Yang, Z.; Li, J.; Guo, Y.; Yang, G.; Yu, Y.; Zhang, J. The advancement of neutron-shielding materials for the transportation and storage of spent nuclear fuel. *Materials* **2022**, *15*, 3255. [CrossRef]
53. Howard, R.H.; Ruggles, A.E. Design and out-of-pile testing of a novel irradiation experiment vehicle to support qualification of nuclear thermal propulsion components. *Nucl. Eng. Des.* **2020**, *361*, 110516. [CrossRef]
54. Şekerci, M.; Özdoğan, H.; Kaplan, A. A study on the cross-section data of 43,44m,46,47Sc isotopes via (d,x) reactions on natural abundance targets under the effects of deuteron optical models. *Appl. Radiat. Isot.* **2023**, *194*, 110717. [CrossRef]

55. Mossini, E.; Revay, Z.; Camerini, A.; Giola, M.; Magugliani, G.; Macerata, E.; Mariani, M. Determination of nuclear graphite impurities by prompt gamma activation analysis to support decommissioning operations. *J. Radioanal. Nucl. Chem.* **2022**, *331*, 3117–3123. [CrossRef]
56. Wang, K.; Ma, L.; Yang, C.; Bian, Z.; Zhang, D.; Cui, S.; Wang, M.; Chen, Z.; Li, X. Recent progress in Gd-containing materials for neutron shielding applications: A review. *Materials* **2023**, *16*, 4305. [CrossRef]
57. Han, I.; Demir, L. Mass attenuation coefficients, effective atomic and electron numbers of Ti and Ni alloys. *Radiat. Meas.* **2009**, *44*, 289–294. [CrossRef]
58. Yilmaz, D.; Şahin, Y.; Demir, L. Studies on mass attenuation coefficient, mass energy absorption coefficient, and kerma for Fe alloys at photon energies of 17.44 to 51.70 keV. *Turk. J. Phys.* **2015**, *39*, 11. [CrossRef]
59. Stettner, C.; Baumgartner, N.; Hranitzky, C.; Poljanc, K.; Stadtmann, H.; Streli, C. A novel approach towards the calculation of dose rate constants for ambient dose equivalent H*(10) by including low energy X-rays. *Appl. Radiat. Isot.* **2021**, *178*, 109964. [CrossRef] [PubMed]
60. Ouaggou, I.A.; Bakari, D.; Rrhioua, A.; Zerfaoui, M.; Oulhouq, Y.; Talbi, M.; Benmessaoud, M. Evaluation of ambient dose equivalent for photoneutrons around linear accelerator and their radioprotection quantities. *Radiat. Phys. Chem.* **2023**, *212*, 111096. [CrossRef]
61. D'Avino, V.; Ambrosino, F.; Bedogni, R.; Campoy, A.I.C.; La Verde, G.; Vernetto, S.; Vigorito, C.F.; Pugliese, M. Characterization of thermoluminescent dosimeters for neutron dosimetry at high altitudes. *Sensors* **2022**, *22*, 5721. [CrossRef]
62. Zehtabvar, M.; Taghandiki, K.; Madani, N.; Sardari, D.; Bashiri, B. A review on the application of machine learning in gamma spectroscopy: Challenges and opportunities. *Spectrosc. J.* **2024**, *2*, 123–144. [CrossRef]
63. Pakari, O.V.; Lucas, A.; Darby, F.B.; Lamirand, V.P.; Maurer, T.; Bisbee, M.G.; Cao, L.R.; Pautz, A.; Pozzi, S.A. Gamma-ray spectroscopy in low-power nuclear research reactors. *J. Nucl. Eng.* **2024**, *5*, 26–43. [CrossRef]
64. Troyanov, V.M.; Toshinsky, G.I.; Stepanov, V.S.; Petrochenko, V.V. Lead-bismuth cooled reactors: History and the potential of development. Part 1. History of development. *Nucl. Energy Technol.* **2022**, *8*, 187–195. [CrossRef]
65. Luoni, F.; Boscolo, D.; Fiore, G.; Bocchini, L.; Horst, F.; Reidel, C.-A.; Schuy, C.; Cipriani, C.; Binello, A.; Baricco, M.; et al. Dose attenuation in innovative shielding materials for radiation protection in space: Measurements and simulations. *Radiat. Res.* **2022**, *198*, 107–119. [CrossRef]
66. Moshkbar-Bakhshayesh, K.; Mohtashami, S. Validation of codes for modeling and simulation of nuclear power plants: A review. *Nucl. Eng. Des.* **2024**, *421*, 113120. [CrossRef]
67. Yokoyama, S.; Hamada, N.; Tsujimura, N.; Kunugita, N.; Nishida, K.; Ezaki, I.; Kato, M.; Okubo, H. Regulatory implementation of the occupational equivalent dose limit for the lens of the eye and underlying relevant efforts in Japan. *Int. J. Radiat. Biol.* **2022**, *99*, 604–619. [CrossRef]
68. Loya, M.; Sanín, L.H.; González, P.R.; Ávila, O.; Duarte, R.; Ojeda, S.L.; Montero-Cabrera, M.E. Measurements of radiation exposure of dentistry students during their radiological training using thermoluminescent dosimetry. *Appl. Radiat. Isot.* **2016**, *107*, 234–238. [CrossRef]

Disclaimer/Publisher's Note: The statements, opinions and data contained in all publications are solely those of the individual author(s) and contributor(s) and not of MDPI and/or the editor(s). MDPI and/or the editor(s) disclaim responsibility for any injury to people or property resulting from any ideas, methods, instructions or products referred to in the content.